A&A 483, 519–527 (2008)
DOI: 10.1051/0004-6361:200809380

Astronomy & Astrophysics

Abundances in planetary nebulae: NGC 6826⋆

R. Surendiranath[1] and S. R. Pottasch[2]

[1] Indian Institute of Astrophysics, Koramangala II Block, Bangalore 560034, India
e-mail: nath@iiap.res.in
[2] Kapteyn Astronomical Institute, PO Box 800, 9700 AV Groningen, The Netherlands
e-mail: pottasch@astro.rug.nl

Received 10 January 2008 / Accepted 29 February 2008

ABSTRACT

Aims. We determine the chemical abundances and other parameters of the nebula NGC 6826 and its central star.
Methods. We present new ISO spectra and combine them with archival IUE and optical spectra from the literature to get a complete, extinction-corrected, spectrum. The chemical composition of the nebula is then calculated in two ways, first by directly calculating and adding individual ion abundances, and second by building a model nebula that will reproduce the observed spectrum.
Results. The results of these two methods are compared. In addition, we discuss the star exciting the nebula.

Key words. ISM: abundances – ISM: planetary nebulae: individual: NGC 6826 – infrared: ISM

1. Introduction

NGC 6826 is an elliptical, almost circular, bright planetary nebula surrounded by a giant circular halo with a radius of about 70″. A pair of irregular knots are located on either side of the nebula, about 12″ from the center. The diameter of the nebula is about 25″. An HST image in visible light is shown as Fig. 1. As can be seen from the figure, there is a smaller, somewhat elliptical structure with a diameter of about 10″ also centered on the central star. This star is quite bright, as seen by the V magnitude of 10.41 given by Acker et al. (1992).

As the PK number indicates, NGC 6826 (PK 083.5+12.7) is somewhat above the galactic plane. Its distance is not well known. Statistical distances are between 0.7 kpc and 1.6 kpc. A distance is computed below by equating the ⟨rms⟩ density with the forbidden line density. A value of $d = 1.1$ kpc is found and used when necessary throughout this paper. This distance is within the above range of the statistical distances; when taken together with the high galactic latitude, this may indicate that the nebula is formed from a low mass star. It is possible that this may be seen in the chemical abundances of the nebula.

The purpose of this paper is to obtain more accurate abundances for this nebula. This is achieved in two ways. The first is by including the ISO spectra. The reasons for this have been discussed in earlier papers (e.g. see Pottasch & Beintema 1999; Pottasch et al. 2006, 2001; Bernard Salas et al. 2001), and can be summarized as follows.

The most important advantage is that the infrared lines originate from very low energy levels and thus give an abundance that is not sensitive to either the temperature in the nebula or to possible temperature fluctuations. Furthermore, when a line originating from a high-lying energy level in the same ion is observed, it is possible to determine an effective electron temperature at which the lines in that particular ion are formed. When the electron temperature for many ions can be determined, it is possible to make a plot of electron temperature against ionization potential, which can be used to determine the effective electron temperature for ions for which only lines originating from a high energy level are observed. Using an effective electron temperature takes into account that ions are formed in different regions of the nebula. At the same time, possible temperature fluctuations are taken into account.

The ISO spectra has further advantages. One of them is that the number of observed ions used in the abundance analysis is

Fig. 1. HST image of NGC 6826; Credits: Bruce Balick, Jason Alexander, Arsen Hajian, Yervant Terzian, Mario Perinotto, Patrizio Patriarchi & NASA.

⋆ Based on observations with ISO, an ESA project with instruments funded by ESA Member States (especially the PI countries: France, Germany, The Netherlands, and the UK) and with the participation of ISAS and NASA.

approximately doubled, which removes the need for using large "ionization correction factors", thus substantially lowering the uncertainty in the abundance. A further advantage is that the extinction in the infrared is almost negligible, eliminating the need to include large correction factors.

The second method of improving the abundances is by using a nebular model to determine them. This has several advantages. First, it provides a physical basis for the electron temperature determination. Second, it permits abundance determination for elements that are observed in only one or a limited number of ionic stages. A further advantage of modeling is that it provides information on the central star and other properties of the nebula.

A disadvantage of modeling is that there are possibly more unknowns than observations, so some assumptions must be made. For example, concerning the geometry, we assume that the nebular is spherical and that no clumping exists. The observed circular form and smooth emission make these assumptions reasonable. Other assumptions are discussed in Sect. 5.

This paper is structured as follows. The spectrum of NGC 6826 is discussed in Sect. 2. Section 3 discusses the simple approach to determining the chemical composition and presents the resulting abundances. In Sect. 4 the abundances are compared with other determinations and the errors involved are discussed. Section 5 deals with the modeling of the PNe and presents the results. This is followed in Sect. 6 by a detailed discussion of the model results concerning the nebular and the central star parameters including a discussion of dust grains present and the accuracies involved in the results. Section 7 briefly dwells on the evolutionary state. Finally, the conclusions are given in Sect. 8.

2. The spectrum of NGC 6826

The ISO SWS observations were made with the SWS02 observing template (see Leech et al. 2004) The SWS02 measurements are more accurate than SWS01 measurements since more time is spent on individual lines. The measurements used, TDT03601952 and TDT04002150, were centered at RA(2000) $19^h44^m48.2^s$ and Dec(2000) +50°31′30.0″, which is very close to the center of the nebula. No SWS01 measurements have ever been made. Data reduction was carried out using ISAP (ISO Spectral Analysis Package) version 2.1. The diaphragm used was 14″ × 20″ below 12 μm and somewhat larger above this wavelength, so that most of the brighter part of the nebula fit within the diaphragm and was measured by the SWS. The amount of flux missed below 12 μm can be found by comparing the Hβ flux derived from the hydrogen lines measured by ISO (8.2×10^{-11} erg cm^{-2} s^{-1}) with the Hβ flux found from the radio frequency measurements (12.8×10^{-11} erg cm^{-2} s^{-1}). This implies that about 35% of the radiation from the nebula was missed below 12 μ. Since the diaphragms above this wavelength are larger, the amount of emission that was missed is smaller. Judging from the fact that IRAS, which measured the entire nebula, found the Ne III 15.55 μm approximately equal to our ISO flux (see Pottasch et al. 1986b), it seems that not much emission has been missed by the ISO diaphragm at this wavelength. Based on the geometry we estimate that only 10% of the radiation was missed above 12 μm.

Seventeen long-wavelength observations were made with the LWS01 template and four with the LWS02 template at essentially the same position, covering the wavelength range from 45 μm to 200 μm. We used the two LWS02 observations TDT13304809 and 86000603, which give very similar results. The diaphragm for the LWS measurements is approximately 80″ in diameter so it includes the entire nebula. The intensities of the lines found in the spectrum are shown in Col. 3 of Table 1. The uncertainty of the stronger lines is less than 10%, while that of the weaker lines could be as much as 30%. No O I lines could be observed in the far infrared, which indicates that any neutral region surrounding the ionized nebula must be small. The C II line at 157.85 μm is uncertain because the background correction is fairly large. The intensities agree reasonably well with those reported by Liu et al. (2004a) for the limited number of lines they observed.

Table 1. ISO observations of NGC 6826 (in units of 10^{-13} erg cm^{-2} s^{-1}).

Ident.	$\lambda(\mu m)$	Intens. (1)	Intens. (2)
H I 6–4	2.626	31.5	3.7
H I 10–5	3.039	6.9:	
H I 9–5	3.297	7.5	0.88
H I 8–5	3.740	8.7	1.02
H I 5–4	4.052	65.	8.5
H I 6–5	7.460	17.8	2.09
[Ar III]	8.992	91.0	10.7
[S IV]	10.510	295.	34.7
[Ne II]	12.813	41.0	4.10
[Ne III]	15.555	1100.	110..
[P III]	17.887	10.	1.0
[S III]	18.713	167.	16.7
[Ar III]	21.837	10.5	1.05
[S III]	33.481	127.	11.6
[Ne III]	36.104	110.	10.0
[O III]	51.833	2170.	170.
[N III]	57.326	408.	31.9
[O III]	88.375	763.	59.6
[C II]	157.851	6.11:	0.48:

Intens. (1) is the average value of the measured intensity. Intens. (2) is the value of the intensity divided by Hβ, where Hβ = 100.
: indicates uncertain value.

2.1. Extinction

For the present purpose, two methods for obtaining the extinction are considered: (1) comparison of radio emission with Hβ flux, and (2) comparison of observed and theoretical Balmer decrement, First, however, we discuss the radio emission and the Hβ flux.

The 6 cm flux density has been measured by several authors and all of them give similar results. We use the value of 375 mJy measured by Gregory & Condon (1991). For comparison Becker et al. (1991) give a value of 373 mJy. Using a value of electron temperature of 9600 K (see below) and a helium abundance determined in a later section, an extinction-corrected Hβ flux of 1.28×10^{-10} erg cm^{-2} s^{-1} is predicted.

The measured Hβ flux listed by Cahn et al. (1992) is 1.09×10^{-10} erg cm^{-2} s^{-1}, which leads to the small value of extinction $C = 0.07$ or $E_{B-V} = 0.05$. The extinction as derived from the Balmer decrement has been found by Liu et al. (2004a) to be $C = 0.06$, which is the same within the errors of each determination. In the remainder of this paper, we use $C = 0.07$, together with the extinction curve of Fluks et al. (1994).

2.2. The visual spectrum

The visual spectrum is taken from the work of Liu et al. (2004a). This spectrum was taken with a long slit that was uniformly moved during the observation so that the entire nebula was

Table 2. Visual spectrum of NGC 6826 (intensities with respect to Hβ = 100).

λ (μm)	Ident.	Meas. Intens.	Unred. Intens.
3726	[O II]	14.3	14.9
3729	[O II]	9.74	10.1
3869	[Ne III]	47.6	49.2
4069	[S II]	0.137	0.141
4076	[S II]	0.171	0.175
4102	H$_\delta$	25.2	25.9
4162	[K V]		0.005
4267	C II	0.562	0.574
4340	Hγ	46.0	46.8
4363	[O III]	3.67	3.74
4471	He I	5.12	5.19
4740	[Ar IV]		0.359
4861	Hβ	100	100
5007	[O III]	756.	753
5518	[Cl II]	0.439:	0.429
5538	[Cl II]	0.400	0.391
5755	[N II]	0.154	0.150
5876	He I	14.8	14.3
6102	[K IV]		0.013
6312	[S III]	0.63	0.60
6563	Hα	290.	277.
6584	[N II]	9.22	8.79
6717	[S II]	0.448	0.426
6731	[S II]	0.612	0.582
7136	[Ar III]	12.2	11.5
7320	[O II]	0.98	0.92
7330	[O II]	0.814	0.765
7531	[Cl IV]	0.043	0.041
9531	[S III]		28.9*

* Hippelein & Munch (1981).

covered. The observed spectrum is therefore an average of the entire nebula. It can thus be directly compared with the ISO and IUE spectra, which are also average values over a large part of the nebula, although not for the entire nebula. For convenience we reproduce the values of intensity given by Liu et al. for those lines that are used in this paper for the abundance determination. In Table 2 the ratio of the intensity to Hβ (Hβ = 100) is given, first directly as measured and second after correcting for reddening. The intensity of λ 5007 is not given by Liu et al., and the value given in the table is three times the intensity of λ4959. The λ 9531 Å intensity is taken from Hippelein & Munch (1981).

2.3. The IUE ultraviolet spectrum

While there are a large number of IUE spectra of this nebula, the diaphragm does not cover the entire nebula so that the total nebular spectrum is difficult to extract. Another difficulty occurs in determining the ratio of the nebular line strength to Hβ. In many nebulae this is done by using the theoretical ratio of the He II lines at λ1640 to λ4686. Unfortunately, the ionization state in this nebula is so low that these two lines are too weak to measure. In the work by Liu et al. (2004a) use is made of the O+2 and N^{+2} ions for which lines exist both in the IUE spectrum and in either the visible or the ISO spectrum. The disadvantage of using these ions is that the theoretical line ratios strongly depend on the electron temperature and density, which can lead to large errors in relating the IUE line strengths to Hβ. An alternative is to relate the visible spectrum to the ultraviolet spectrum using the O II lines λ7325 and λ2471. These lines are both doublets

Table 3. IUE spectrum of NGC 6826.

λ	Ion	Meas. Intens.*	Unred. Intens./H$\beta^\dagger$
1335	C II	9.57	3.95
1663	O III]	5.17	2.13
1750	N III]	4.05	1.67
1761	C II	6.93	2.86
1881	Si III]	4.35	1.79
1890	Si III]	2.91	1.20
1906	C III]	120.	49.5
1909	C III]	81.6	33.7
2325	C II]	7.85	3.24
2471	[O II]	3.09	1.27
2832	He I	4.62	1.91
2944	He I	4.64	1.91

* Units: 10^{-13} erg cm^{-2} s^{-1}, † Hβ = 100.

arising from the same upper levels, which have very nearly the same energy, so their ratio is almost independent of both electron temperature and density. For the range of temperatures and densities in this nebula, the value of the ratio λ2471/λ7325 = 0.754. Combining this with the λ7325 shown in Table 2, a value of the ratio λ2471/Hβ = 1.27×10^{-2} is predicted. Combining this with an extinction-corrected total Hβ flux of 1.28×10^{-10} predicts an extinction-corrected value of the doublet λ2471 = 1.63×10^{-12}. The value we measured in the high-resolution LWP07727 spectrum is 3.09×10^{-13}; thus a factor of 5.28 must be applied to go from the measured spectrum to the total extinction-corrected nebular flux. Since this extinction correction is at λ2471, a correction for reddening relative to this wavelength must be applied to the other lines, but this correction is relatively small. The results are given in Table 3, where the third column is the measured IUE line intensity and the fourth column is the extinction-corrected line flux relative to Hβ. The measurements in Table 3 were found as follows. The lines below 1900 Å were taken as the average of the SWP06258 and SWP14626 spectra. Those on the longwave side are the average of LWR11207, LWR11215, and LWR10541. The C III lines were measured in the high resolution SWP20869 spectrum.

3. Chemical composition of NGC 6826 from simplified analysis

This method of analysis is the same as in the papers cited in the introduction. First, the electron density and temperature are determined as a function of the ionization potential are determined. Then the ionic abundancesare determined, using the density and temperature appropriate for the ion under consideration, together with Eq. (1). Then the element abundances are found for those elements in which a sufficient number of ions abundances have been derived.

3.1. Electron density

The ions used to determine N_e are listed in the first column of Table 4. The ionization potential required to reach that ionization stage, and the wavelengths of the lines used, are given in Cols. 2 and 3 of the table. Note that the wavelength units are Å when 4 ciphers are given and microns when 3 ciphers are shown. The observed ratio of the lines is given in the fourth column and the corresponding N_e in the fifth column. The temperature used is discussed in the following section, but is unimportant since these line ratios are essentially determined by the density.

Table 4. Electron density indicators in NGC 6826.

Ion	Ioniz. pot. (eV)	Lines used	Observed ratio	N_e (cm^{-3})
[S II]	10.4	6731/6716	1.37	1900
[O II]	13.6	3626/3729	1.50	2200
[S III]	23.3	33.5/18.7	0.70	1400
[Cl III]	23.8	5538/5518	0.91	1600
[C III]	24.4	1906/1909	1.47	1600
[O III]	35.1	51.8/88.4	2.87	1350
[Ar IV]	40.7	4740/4711	0.93	2200

Table 5. Electron temperature indicators in NGC 6826.

Ion	Ioniz. pot. (eV)	Lines used	Observed ratio	T_e (K)
[N II]	14.5	5755/6584	0.0171	9900
[S III]	23.3	6312/18.7	0.036	9100
[S III]	23.3	9531/18.7	1.73	9600
[Ar III]	27.6	7136/8.99	1.075	9400
[N III]	29.6	1750/57.3	0.053	8900
[O III]	35.1	4363/5007	0.00498	9350
[O III]	35.1	1663/5007	0.00283	8600
[O III]	35.1	5007/51.8	4.43	8550
[Ne III]	41.0	3868/15.5	0.447	9100

The electron density appears to be about 1700−2000 cm^{-3}. There is no indication that the electron density varies with ionization potential in a systematic way. It is interesting to compare this value of the density with the ⟨rms⟩ density found from the Hβ line. This depends on the distance of the nebula, which is not known accurately, and on the angular size of the nebula. Because of the distance uncertainty, we turn the calculation around and compute what the distance will be for an ⟨rms⟩ density of 2000 cm^{-3} in a sphere of radius 12.5″, which emits the Hβ flux given above. This yields a distance of 1.1 kpc. While this is a reasonable distance, it is very uncertain. Nevertheless, this value will be used in further computations in this paper.

3.2. Electron temperature

A number of ions have lines originating from energy levels far enough apart that their ratio is sensitive to the electron temperature. These are listed in Table 5, which is arranged like the previous table. The electron temperature is found to be roughly constant as a function of ionization potential. There is some scatter and the average temperature is about 9100 K.

3.3. Ionic and element abundances

The ionic abundances were determined using the equation

$$\frac{N_{ion}}{N_p} = \frac{I_{ion}}{I_{H_\beta}} N_e \frac{\lambda_{ul}}{\lambda_{H_\beta}} \frac{\alpha_{H_\beta}}{A_{ul}} \left(\frac{N_u}{N_{ion}}\right)^{-1} \quad (1)$$

where I_{ion}/I_{H_β} is the measured intensity of the ionic line compared to Hβ, N_p is the density of ionized hydrogen, λ_{ul} the wavelength of this line, λ_{H_β} the wavelength of Hβ, α_{H_β} the effective recombination coefficient for Hβ, A_{ul} the Einstein spontaneous transition rate for the line, and N_u/N_{ion} the ratio of the population of the level from which the line originates to the total population of the ion. This ratio has been determined using a five-level atom.

The results are given in Table 6, where the first column lists the ion concerned, and the second column the line used for the abundance determination. The third column gives the intensity of the line used relative to Hβ = 100. The fourth column gives the ionic abundances, and the fifth the ionization correction factor (ICF). This has been determined empirically, with the help of the model discussed below. Notice that the ICF is usually unity and the element abundances, given in the last column, are probably well determined. The abundance of C^{+3} cannot be determined because the nebular lines at λ1548 Å are difficult to separate from lines formed in the stellar wind. In determining the abundances a constant density of $N_e = 2 \times 10^3$ and an electron temperature of 9100 K has been used.

Table 6. Ionic concentrations and chemical abundances in NGC 6826. Wavelength in angstrom for all values of λ above 1000, otherwise in μm.

Ion	λ	Intens./Hβ	N_{ion}/N_p	ICF	$N_{el.}/N_p$
He^+	5875	14.3	0.095	1	0.95
C^+	2325	3.24	1.15(–5)		
C^{++}	1909	83.2	4.32(–4)	1.2	5.3(–4)
N^+	6584	8.79	2.16(–6)		
N^{++}	1750	1.67	2.63(–5)		
N^{++}	57.3	49.8	5.69(–5)	1	5.0(–5)
O^+	3726	14.9	1.8(–5)		
O^{++}	5007	753.	3.72(–4)		
O^{++}	51,8	265.	2.82(–4)	1	4.0(–4)
Ne^+	12.8	4.1	6.33(–6)		
Ne^{++}	15.5	110.	7.23(–5)		
Ne^{++}	3869	49.2	2.23(–4)	1	1.5(–4)
S^+	6731	0.582	3.7(–8)		
S^{++}	6312	0.604	1.96(–6)		
S^{++}	18.7	16.7	1.59(–6)		
S^{+3}	10.5	34.7	9.1(–7)	1	2.8(–6)
Ar^{++}	8.99	10.6	1.07(–6)		
Ar^{++}	7136	11.3	1.31(–6)		
Ar^{+3}	4740	0.36	1.6(–7)	1	1.4(–6)
Cl^{++}	5538	0.391	7.56(–8)		
Cl^{+3}	7531	0.041	1.09(–8)	1	9.0(–8)
K^{+3}	6101	0.013	1.5(–9)		
K^{+4}	4163	0.005	1.5(–9)	1:	3.0(–9):
P^{++}	17.8	1.22	8.3(–8)	2:	1.7(–7)
Si^{++}	1890	2.99		1	

Intensities given with respect to Hβ = 100.

The abundances in NGC 6826 are in general similar to solar abundances. This is shown in Table 7 where it can be seen that the abundances of oxygen, nitrogen, and neon agree and are similar to those of the sun. Sulfur is lower than solar, but it is lower in most nebulae and it is likely that the solar abundance is anomalous. Carbon is the only element with a higher abundance: a factor of two above solar. Iron, and to a lesser extent silicon, chlorine, and argon, are depleted with respect to the solar value. Iron has been seen to be depleted in all nebulae in which it has been measured, and this is presumably due to depletion onto dust grains.

4. Comparison with other abundance determinations

Table 7 is a comparison of the abundances with the most important determinations in the past 20 years. There is marginal agreement, usually to within a factor of two. A comparison is also made with the solar abundance (Asplund et al. 2005; except for neon and argon, which are taken from the discussion of Pottasch & Bernard-Salas 2006).

Table 7. Comparison of abundances in NGC 6826.

Elem.	Present	Model	Liu (1)	Barker (2)	Solar (3)
He	0.095	0.11		0.094	0.098
C(–4)	5.3	4.33	2.9	3.4	2.5
N(–4)	0.50	0.66	0.69	0.51	0.60
O(–4)	4.0	3.85	3.3	4.0	4.6
Ne(–4)	1.5	0.8	0.66	0.92	1.2
Si(–6)		4.32			32.
P(–7)	1.7	2.4			2.3
S(–6)	2.8	2.38	2.4	5.9	14
Cl(–8)	9.0	8.0	7.8		31.
Ar(–6)	1.4	1.3	0.98	1.3	4.2
Fe(–7)		6.1	3.8		280

(1) Liu et al. (2004a); (2) Barker (1988); (3) Solar: Asplund et al. (2005). The numbers in parentheses in the first column are the powers of 10 by which the other columns are to be multiplied.

The helium abundance was derived using the theoretical work of Benjamin et al. (1999). For recombination of singly ionized helium, most weight is given to the λ 5875Å line, because the theoretical determination of this line is the most reliable.

4.1. Errors

It is difficult to determine the errors in the abundance determination. This is because the error can occur at several stages in the determination. An error can occur in the intensity determination, which can be specified as probably less than 30% and may be lower for the stronger lines. An error may occur in correcting for the extinction, either because the extinction is incorrect or the average reddening law is not applicable. We tried to minimize this possibility by making use of known atomic constants to relate the various parts of the spectrum. Thus the ratio of the infrared spectrum to the visible spectrum is fixed by the ratio of Brα to Hβ, which varies only slightly with nebular temperature and density.

Another error is introduced by the correction for unseen stages of ionization. This varies with the element, but is usually small because many ionization stages are observed. Thus all but neutral neon is observed, so that the error for neon is negligible. This is also true for sulfur, argon, oxygen, and nitrogen where the higher stages of ionization that are not observed contribute little to the abundance.

There is also an error due to incorrect determination of the electron temperature. This is very small for ions represented by infrared lines, so that the abundances of neon, argon and sulfur, will not be affected. The abundance of carbon is more sensitive to the temperature, however, so that an error of 200 K could have a substantial effect.

4.2. Recombination line abundances

Liu et al. (2004a) discuss the recombination line abundances in NGC 6826 for several ions of carbon, nitrogen, oxygen, and neon using their careful measurements of very weak lines from this nebula. These abundances are about 50% higher for oxygen and neon than those we obtained from the collisional lines. Our carbon results agree with the recombination line determination for this element. The only difference that seems greater than the errors involved occurs for nitrogen for which the recombination line abundance is a factor of 3 to 4 higher than we have found. The various recombination lines of N^{++} Liu et al., however, use give a range of nitrogen abundances covering a factor of 3.5. Because Liu et al. find somewhat lower collisional line abundances, their differences between collisional and recombination line abundances is somewhat larger.

5. Model

To obtain as nearly correct a model as possible, both the star and the nebula must be considered. Let us first consider the star. There are several ways to obtain a reasonable estimate of the stellar temperature.

Modeling the nebula-star complex will allow for characterizing not only the central star's temperature but also other stellar parameters (i.e., log g and luminosity). It can determine distance and other nebular properties, especially the composition, including the composition of elements that are represented by a single stage of ionization, which cannot be determined by the simplified analysis above. This method can take into the presence of dust and molecules, if any, into account in the nebular material, so it is very comprehensive in approach. While the line ratio method is simple and fast, the ICFs rest on uncertain physics. To this end, modeling serves as an effective method, and the whole set of parameters is determined in an unified way, assuring self consistency. Also, this way one gets a good physical insight into the PN, the method, and the observations. Thus, modeling is a good approach for an end-to-end solution to the problem.

It is with this in mind that we constructed a photoionization model for NGC 6826 with the code Cloudy, using the latest version C07.02.01 (Ferland et al. 1998). One of the highlights of this version has been some major revisions in the atomic data used. More information on this can be found on Cloudy's website.

5.1. Assumptions

From the available HST image of this PN, we found that the nebula is nearly spherical, so we use a spherical geometry for our modeling. But the image also indicates that the density is not uniform, so we used a density profile derived for this nebula by Plait & Soker (1990) from CCD images in Hα. These authors deconvolved the density from the emission measure, and we used the radial density profile given by them in Fig. 3 of their paper. The density at about 20 arcsec distance from the center is about 140 cm^{-3}, and we took this fiducial point as the outer edge in our model. In the deconvolution process, spherical symmetry has been assumed by them. We ignore the two symmetrically placed blobs of gas seen near the outer edge of the nebular image. Later we modified this profile in the modeling process (see below). We included dust grains mixed with gas in the nebula, so that we could compare model dust-grain emission continua with the ISO observations. To represent the central star's emission, we experimented with several model atmospheres available within the in-built library of Cloudy.

5.2. Results

The general method of applying the code Cloudy to model NGC 6826 is the same as in Surendiranath et al. (2004). We ran a number of models, and each time the output was carefully scrutinized before running the next model with changed input parameters. We tried to match the observed spectral fluxes of about 70 lines and relied on physical intuition rather than any of the optimization techniques provided in Cloudy. The results

Table 8. Parameters representing the best-fit model.

Parameter	Value
Ionizing source	
Model atmosphere	Tlusty
$T_{\rm eff}$	47 500 K
Log g	3.75
Luminosity	1640 $L_\odot$
Nebula	
Density profile	See Fig. 2
Abundance	H He C N 12.000 11.041 8.637 7.820 O Ne Si P 8.586 7.903 6.636 5.380 S Cl Ar Fe 6.377 4.903 6.114 5.784
Size	20″ (radius)
Distance	1.40 kpc
Dust grains	Silicates of single size 0.01 μm; see Fig. 5
Inner radius	6.283e15 cm (~0.00203 pc)
Outer radius	4.189e17 cm (~0.136 pc)
Filling factor	1.0

are presented essentially in Tables 8 and 9 and discussed in more detail in the following section.

6. Discussion

The best-fit model input parameters are our final values for the characteristics of the nebula and its central star (see Table 8).

6.1. Nebular density and temperature

The nebular density profile that was applied to the final model is shown in Fig. 2 (continuous curve). We deviated from the density profile given by Plait & Soker (1990) in their Fig. 3. In the final model, the value of N(H) at each radial point is up by 26.5% relative to the value given by Plait & Soker. We also treated distance as a variable parameter, and any change in distance gets reflected in a change in the model input density profile because the abscissae points of the profile by Plait & Soker are radial angular distances. The original profile is shown by symbols at selected abscissae points in Fig. 2 for a distance of 1.4 kpc. At 0.3 and 0.6 arcsec, we assumed values of 1900 cm^{-3} and 1700 cm^{-3}, respectively, while interpolating the original profile. The electron density $N_{\rm e}$, and electron temperature $T_{\rm e}$ of the final model are plotted against the nebular depth in Fig. 3. It can be seen that these values are in good agreement with those determined by line ratios and presented in Tables 4 and 5.

6.2. Comparison of the model spectrum with observation

The final model and the observed spectral line fluxes are listed in Table 9. The absolute Hβ flux matches the observation very well. The agreement is generally good for other lines, barring some in which the model line fluxes deviate by a large amount. We do not understand the reason for the deviation of [O II] blue lines at 3727 and 3729, while its red lines 7323 and 7332 fit better. The C II 1335, 1761 and 157.6 μm, and [S IV] 10.51 μm also show large deviations. We note that neon lines in the model are behaving well and are close to the observations. We never had such agreement for the case of neon in our earlier modeling of several nebulae in this series of papers. We would like to highlight one important aspect, namely the variability of the spectrum of the PN due to a variable stellar wind that is known for this PN. We have assembled different spectra of different wavelength regions, each observed at a different epoch of time. Thus the cause of the above-mentioned discrepancies may be these, at least in part. Other causes could be the somewhat arbitrary dust grain abundance distribution (across the nebula), which we adopted (Fig. 5) to get a good fit, and the uncertainties involved in the flux measurements of weaker lines in ISO spectra. We note that the accuracy of the optical spectrum used in this analysis (a few times 10^{-4} of H$_\beta$) is rather high compared to the IUE and ISO spectra that were used. But we expect that our determined parameters would not be affected much since the overall error estimate for each of them is around 25%.

6.3. The central star

We have experimented with a number of different model atmospheres to represent the ionizing flux from the central star. We only used the original shape of the model atmosphere continuum but varied the luminosity as facilated by Cloudy. To begin with, as the central star is known to exhibit winds, we tried the WMbasic windy model atmospheres of Pauldrach et al. (2001). As we could not get satisfactory results with these, we also experimented with the model atmospheres of Rauch (2003) and Tlusty models of Lanz & Hubeny (2003). These two are static models. Our final model incorporates the Tlusty model atmospheres with the characteristics listed in Table 8 and is found to reproduce the observed spectral fluxes. Figure 4 shows the incident and transmitted fluxes of the model central star (CSPN) atmosphere. "Incident" refers to the stellar photospheric flux hitting the inner edge of the nebula and "Transmitted" refers to how much of this passes through unabsorbed by the nebula between the inner and the outer edge. The transmitted flux seems to be quite high. The final transmitted flux (not shown above) at any frequency is the above one plus whatever is generated by gas and dust within the nebula in both the line and the contiuum. In general we always try to conserve the flux and experiment with models that could make the transmitted flux a minimum.

6.3.1. Luminosity, mass and distance

Recently, Pauldrach et al. (2004) have determined the CSPN parameters for NGC 6826 using model atmosphere analysis. It is insightful to to compare our determinations with these. Our best-fit model luminosity is 1640 $L_\odot$, whereas they list the very different value of 15 850 $L_\odot$. And we have already showed that the transmitted flux is high even with our lower value of luminosity. They give a mass of 1.40 $M_\odot$ and also computed a distance of 3.18 kpc by a method described by Méndez et al. (1992), using stellar mass, log g, monochromatic model atmosphere flux at visual wavelength, and dereddened apparent visual magnitude. By using their distance and using the original density profile of Plait & Soker (1990), we get (by volume integrating for the size of 20 arcsec) a value of 2.35 $M_\odot$ for the nebular mass, whereas using our best-fit PN model values, we get the more realistic value of 0.25 $M_\odot$ even though our density profile had enhanced values of density relative to the original (see Fig. 2). This means that the case for a larger distance of 3.18 kpc and core mass of 1.40 $M_\odot$ is ruled out.

Our final model CSPN's $T_{\rm eff}$ and log g agree reasonably with those determined by Pauldrach et al. (2004), but the luminosity given by them (15 850 $L_\odot$) is much too high compared to our

Table 9. The emission line fluxes (Hβ = 100).

Label	Line	Model flux	Obs. flux (dereddened)	Label	Line	Model flux	Obs. flux (dereddened)
TOTL	4861 A	100.00	100.00	N 2	5755 A	0.13	0.15
C 2	1335 A	23.60	3.95	He 1	5876 A	13.76	14.34
TOTL	1665 A	3.09	2.13	O 1	6300 A	0.02	0.07
TOTL	1750 A	2.20	1.67	S 3	6312 A	0.55	0.60
C 2	1761 A	0.36	2.86	N 2	6548 A	3.39	3.04
Si 3	1883 A	1.89	1.79	N 2	6584 A	10.00	8.79
Si 3	1892 A	1.19	1.20	He 1	6678 A	3.69	4.07
TOTL	1909 A	85.94	82.80	S II	6716 A	0.56	0.43
TOTL	2326 A	5.74	3.24	S II	6731 A	0.68	0.58
O II	2471 A	1.12	1.27	He 1	7065 A	6.77	3.94
He 1	2829 A	1.12	1.91	Ar 3	7135 A	10.50	11.51
He 1	2945 A	1.86	1.91	O II	7323 A	0.83	0.92
He 1	3614 A	0.70	0.62	O II	7332 A	0.66	0.77
H 1	3687 A	0.64	0.83	Ar 3	7751 A	2.53	2.71
H 1	3692 A	0.72	0.97	S 3	9532 A	25.19	28.90
O II	3726 A	23.82	14.85	H 1	2.625 m	4.76	3.70
O II	3729 A	17.28	10.11	H 1	3.296 m	0.80	0.88
Ne 3	3869 A	53.74	49.24	H 1	3.740 m	1.14	1.02
He 1	3965 A	1.35	1.14	H 1	4.051 m	8.48	8.50
Ne 3	3968 A	16.20	14.34	H 1	7.458 m	2.74	2.09
He 1	4026 A	2.51	2.37	Ar 3	9.000 m	10.23	10.70
H 1	4102 A	26.46	25.88	S 4	10.51 m	24.55	34.70
H 1	4340 A	47.28	46.82	Ne 2	12.81 m	6.82	4.10
TOTL	4363 A	3.95	3.74	Ne 3	15.55 m	98.78	110.00
Fe 2	4416 A	0.00	0.05	P 3	17.89 m	0.91	1.00
Fe 3	4659 A	0.14	0.14	S 3	18.67 m	17.89	16.70
Fe 3	4755 A	0.02	0.07	Ar 3	21.83 m	0.69	1.05
Ar 4	4711 A	0.46	0.39	S 3	33.47 m	12.87	11.60
Ar 4	4740 A	0.41	0.36	Si 2	34.81 m	1.00	≤2.0
Fe 3	4881 A	0.03	0.06	Ne 3	36.01 m	8.56	10.00
O 3	4959 A	254.82	251.10	O 3	51.80 m	162.25	170.00
Fe 3	5271 A	0.08	0.06	N 3	57.21 m	28.11	31.90
Cl 3	5518 A	0.41	0.43	O 3	88.33 m	56.17	59.60
Cl 3	5538 A	0.36	0.39	C 2	157.6 m	0.26	0.48

Absolute Hβ flux(n.lobe) Model: 1.29×10^{-10} erg cm^{-2} s^{-1} Obsn: 1.28×10^{-10} erg cm^{-2} s^{-1}.
Notes: "A" in Col. "Line" signifies angstrom; "m" signifies μm. In Col. "Label", we have followed the notation used by Cloudy for atoms and ions; this will make identifying a line in Cloudy's huge line list easy. Neutral state is indicated by "1" and singly ionized state by "2" etc., "TOTL" typically means the sum of all the lines in the doublet/multiplet; or it could mean sum of all processes: recombination, collisional excitation, and charge transfer. Some elements are represented by usual notation as per Cloudy.

determination of 1640 $L_\odot$. There are two ways this can be counterchecked. First, we ran a model with $T_{\rm eff}$ = 44 000 K, log g = 3.90, L = 15 000 $L_\odot$ and distance = 3.18 kpc with the Tlusty model atmosphere. This model had the original density profile of Plait & Soker (1990). The predicted absolute H$_\beta$ flux was nearly 1.5 times the observed value. There was no good match between model line fluxes and observed line fluxes. This test model's dust IR continuum was very high compared to ISO observations, so a very high value of 15 000 $L_\odot$ and a distance of 3.18 kpc do not seem to fit in with observations from a modeling point of view.

Second, we measured the observed continuum at 930 Å from FUSE (Far Ultraviolet Spectroscopic Explorer) spectrum of NGC 6826, which was centered on the star (Data ID = P1930401000) to be 2.2×10^{-11} erg cm^{-2} s^{-1} Å^{-1}. From our best-fit model, this flux is 1.74×10^{-11} erg cm^{-2} s^{-1} Å^{-1}. Another measurement was made at 1247 Å from the IUE spectrum used in this paper. This was 2.75×10^{-13} erg cm^{-2} s^{-1} Å^{-1}, and from our model we have 8.75×10^{-12} erg cm^{-2} s^{-1} Å^{-1}. Thus our best-fit model transmits more at IUE wavelengths, while it is in agreement at FUSE wavelengths. These two arguments strongly rule out a higher luminosity than given by us. The FUSE spectrum was processed by using STSDAS and IRAF packages. We note that we only did a preliminary analysis of two other FUSE spectra that were centered on the nebula. Because of this, as well as the general lack of availability of far UV lines in the FUSE range with good atomic data in Cloudy, for practical reasons, we excluded these FUSE nebular spectra in our work.

6.4. Fuse spectra

Fuse spectra centered on the nebula alone were retrieved from the FUSE archive (http://archive.stsci.edu/fuse). The spectra with the Data IDs D1200601000 and D1201601000, cover the range 915 Å through 1180 Å and have a resolution of about 0.08 Å. Quite a few nebular lines are seen, the strongest belonging to S III, C III, and P III, but S IV, Fe III, and possibly N III are also seen. We originally attempted to incorporate these spectra into the present analysis but this proved too difficult. The main source of the difficulty is the comparison of the abundance determined from these lines to hydrogen. No reliable hydrogen lines are found in the spectra. We thought of using the nebular continuum but found that it had too high an intensity to be caused

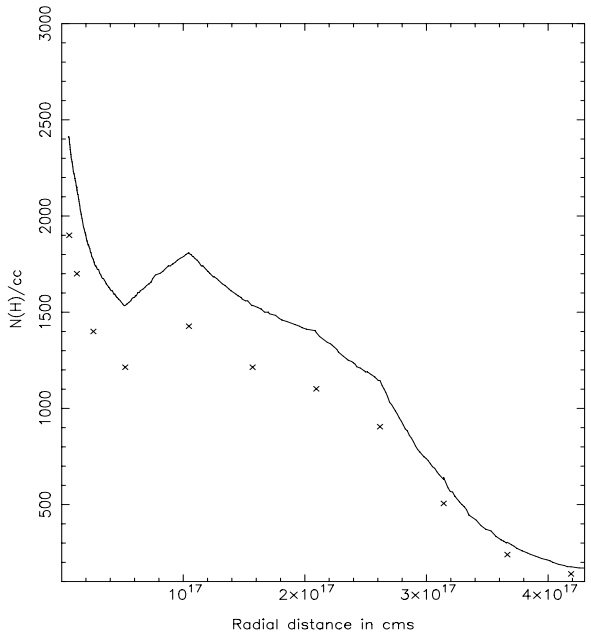

Fig. 2. The symbols represent the density profile by Plait & Soker for 1.4 kpc, while the upper curve represents the adopted profile in the final model.

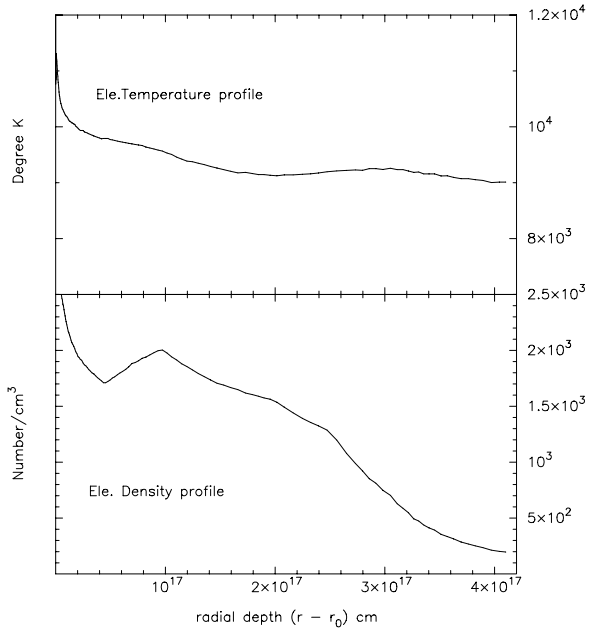

Fig. 3. The inner radius of the nebula is r_o. r is the radial distance from the central star.

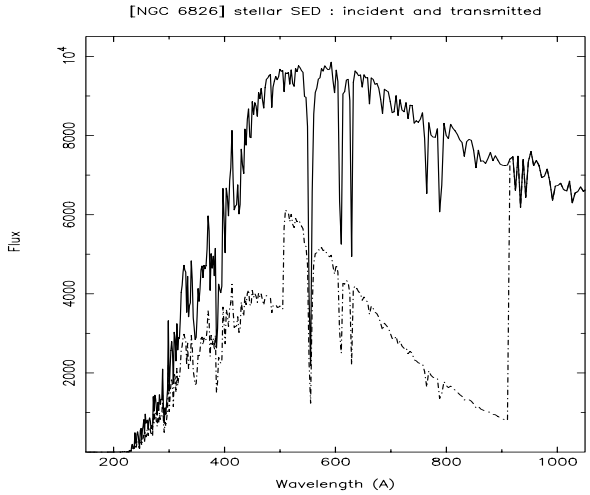

Fig. 4. *Upper curve*: the incident stellar radiation from the model atmosphere whose parameters are given in Table 8. *The lower curve* is the stellar radiation that passes unabsorbed through the nebula to its outer edge.

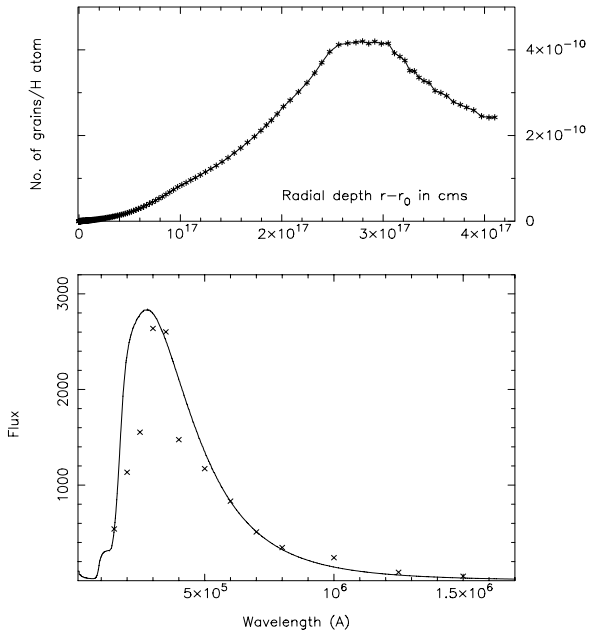

Fig. 5. *Upper curve*: the dust grain abundance distribution; *the lower*: the model IR continua compared to the ISO observations (symbols) as discussed in Sect. 2.

by atomic processes involving hydrogen and helium ions and electrons. We suspect that stellar continuum is being scattered into the observed spectrum probably in the telescope. Because of this and the lack of atomic data for many lines, we did not carry out any further analysis. We point out that these spectra are also interesting because of the interstellar absorption lines found together with strong absorption lines of the H_2 molecule, which is surprising because of the very low extinction in the line of sight. We crosschecked with the ORFEUS (Orbiting and Retrievable Far and Extreme Ultraviolet Spectrometer) spectrum of this object and found the H_2 lines there as well.

6.5. Dust

We included silicate dust grains of a single size (0.01 μm) in the model in order to reproduce the observed continuum in the ISO spectra. Though the extinction to this object is very small, the IRAS fluxes and the ISO observations indicated that some amount of cool (~50–60 K) dust grains are present in the nebula. After some experimentation we varied the quantity of dust to get a good fit to the observations. The variation in the grain abundance across the nebula follows the law, $A = n(\mathrm{H}^\circ)/n(\mathrm{H_{tot}})$, where A is the factor proportionate to which an arbitrarily fixed quantum is varied. Figure 5 shows the details. The upper part gives the number of grains per hydrogen atom across the nebula and the lower part shows the emitted dust IR continua

(continuous curve) and the observed ISO continua (symbols). The model flux is seen to be somewhat higher at lower wavelengths. Since the ISO spectra did not give us any clear indication of a carbon-rich dust, we did not experiment with carbon grains. Carbon grains have higher emissivity than silicates. The model predicted C/O ratio of greater than unity is not to be taken very seriously as the error quoted above indicates. The mean dust-to-gas ratio by mass is ≈0.0012, which gives a very low total dust mass of about 0.0003 $M_{\odot}$, and the visual extinction suffered within the nebula is less than 0.002 mag.

7. Evolutionary state

The helium abundance found for NGC 6826 is very close to the solar value. This indicates that very little helium has been formed in the course of its evolution, which places a maximum value of about 2 $M_{\odot}$ on the original mass of the central star. Of the 30 PNe for which abundance analyses have been carried out with the help of mid-infrared observations, about 10 have approximately solar helium abundance. These nebulae also have an elliptical morphology. More surprising is the rather low nitrogen abundance of this nebula, which is also very close to solar: little or no nitrogen has been formed in the course of the evolution of this nebula. Only two other PNe, which have been studied in the mid-infrared, have not produced nitrogen in the course of evolution: the nearby bright nebula NGC 7662 and the faint smaller nebula Me 2-1. All three nebulae show very similar abundances to that of the Sun. All three nebulae are also found at rather high galactic latitudes. This indicates that the initial mass of all three nebulae must have been very low indeed, in the order of 1 $M_{\odot}$.

8. Conclusions

We have presented the ISO spectra of NGC 6826 and determined its abundances by both the ICF method and by modeling. It can be seen that these two determinations compare well (Table 7). In addition, we could determine the parameters of the central star, and these ($T_{\rm eff}$ and log g) agree with the earlier determination from model atmosphere analysis. We have shown how our determinations of luminosity and distance are physically more reliable compared to the determinations of Pauldrach et al. (2004) and Kudritzki et al. (1997). Our values are considerably lower, and are in agreement with the arguments given by Napiwotzki (2006). This demonstrates the importance and the power of the modeling methodology, which can not only determine improved nebular abundances, but but can also give indications of the CSPN luminosity and distance.

Acknowledgements. We acknowledge the use of SIMBAD and ADS in this research work. R.S. would like to thank J. S. Nathan and B. A. Varghese for their help with software upgradation/installation, and express gratitude for clarifications regarding STSDAS from the helpdesk at STSCI (Phil Hodge). Use has been made of the multiple archive MAST at STSCI.

Note added in proof: The measured continua at 930 Å and 1247 Å mentioned in Sect. 6.3.1 were not dereddened before comparing with model values introducing some error. If dereddened they would be higher by a factor ∼2 and 1.30 respectively.

References

Acker, A., Marcout, J., Ochsenbein, F., et al. 1992, Strasbourg-ESO catalogue
Aller, L. H., & Czyzak, S. J. 1979, Ap&SS, 62, 397
Asplund, M., Grevesse, N., & Sauval, A. J. 2005, ASP Conf. Ser., ed. Bash & Barnes
Barker, T. 1988, ApJ, 326, 164
Becker, R. H., White, R. L., & Edwards, A. L. 1991, ApJS, 75, 1
Benjamin, R. A., Skillman, E. D., & Smits, D. P. 1999, ApJ, 514, 307
Bernard Salas, J., Pottasch, S. R., Beintema, D. A., & Wesselius, P. R. 2001, A&A, 367, 949
Cahn, J. H., Kaler, J. B., & Stanghellini, L. 1992, A&AS, 94, 399
Condon, J. J., & Kaplan, D. L. 1998, ApJS, 117, 361
Davey, A. R., Storey, P. J., & Kisielius, R. 2000, A&AS, 142, 85
Ferland, G. J., Korista, K. T., Verner, D. A., et al. 1998, PASP, 110, 761
Fluks, M. A., Plez, B., de Winter, D., et al. 1994, A&AS, 105, 311
Gathier, R., & Pottasch, S. R. 1988, A&A, 197, 266
Gregory, P. C., & Condon, J. J. 1991, ApJS, 75, 1011
Gregory, P. C., Vavasour, J. D., Scott, W. K., et al. 1994, ApJS, 90, 173
Griffith, M. R., Burke, B. F., & Ekers, R. D. 1994, ApJS, 91, 111
Hippelein, H., & Munch, G. 1981, A&A, 95, 100
Hummer, D. G., & Storey, P. J. 1987, MNRAS, 224, 801
Kingsburgh, R. L., & Barlow, M. J. 1994, MNRAS, 271, 257
Kudritzki, R. P., Méndez, R. H., Puls, J., et al. 1997, IAU Symp., 180, 64
Lanz, T., & Hubeny, I. 2003, ApJS, 146, 417
Leech, J. 2004, MNRAS, 353, 1231
Liu, Y., Liu, X.-W., Luo, S.-G., & Barlow, M. J. 2004a, MNRAS, 353, 1231
Liu, Y., Liu, X.-W., Barlow, M. J., & Luo, S.-G. 2004b, MNRAS, 353, 1251
Méndez, R. H., Kudritzki, R.-P., & Herrero, A. 1992, A&A, 260, 329
Napiwotzki, R. 2006, A&A, 451, L27
Pauldrach, A. W. A., Hoffmann, T. L., & Lennon, M. 2001, A&A, 375, 161
Pauldrach, A. W. A., Hoffmann, T. L., & Mendez, R. H. 2004, A&A, 419, 1111
Plait, P., & Soker, N. 1990, AJ, 99, 1883
Pottasch, S. R., & Acker, A. 1989, A&A, 221, 123
Pottasch, S. R., & Beintema, D. A. 1999, A&A, 347, 974
Pottasch, S. R., & Bernard-Salas, J. 2006, A&A, 457, 189
Pottasch, S. R., Wesselius, P. R., Wu, C. C., et al. 1977, A&A, 54, 435
Pottasch, S. R., Dennefeld, M., & Mo, J.-E. 1986a, A&A, 155, 397
Pottasch, S. R., Preite-Martinez, A., Olnon, F. M., et al. 1986b, A&A, 161, 363
Pottasch, S. R., Beintema, D. A., Bernard Salas, J., & Feibelman, W. A. 2001, A&A, 380, 684
Pottasch, S. R., Beintema, D. A., Bernard Salas, J., et al. 2002, A&A, 393, 285
Preite-Martinez, A., & Pottasch, S. R. 1983, A&A, 126, 31
Rauch, T. 2003 A&A, 403, 709
Surendiranath, R., Pottasch, S. R., & García-Lario, P. 2004, A&A, 421, 1051